ADVANCED MATERIALS INTERFACES
Open Access
www.advmatinterfaces.de

Enhancing Environmental Stability and Transparency of Glass Coatings Using Silica Nanoparticles in the Sol-Gel Process

Giulia Franceschin, Stefano Centenaro, Matteo Lorenzoni, Riccardo Carzino, Luca Ceseracciu, Simone Lauciello, Elti Cattaruzza, and Arianna Traviglia**

Sol-gel technology has long been recognized as a promising stabilization treatment for glass. However, the acidity of its formulations may pose challenges, particularly due to the potential for corrosive effects, making its application on ancient and artistic glass more complex and requiring a delicate balance between safeguarding its structural integrity and preserving its visual and historical significance. This study investigates the incorporation of silica nanoparticles into silica-based coatings to reduce the synthesis acidity and enhance anticorrosion protection. The sol-gel formulations, tailored to minimize their acidity (from pH 1–2 to pH 4) and ensure optimal compatibility with glass surfaces, are combined with 50nm and 200nm silica nanoparticles and applied using dip-coating. Comprehensive analyses, including optical characterization, water contact angle measurements, and nanoindentation tests, reveals that composite coatings with 50nm nanoparticles, applied through a double-dipping process, significantly improves resistance to alteration. These coatings demonstrates superior protective performance compare to both pure silica coatings and composite compositions containing 200nm nanoparticles. Surface analyses further highlighted that incorporating nanoparticles allowed for precise control over the formation of alteration structures on glass surfaces. This approach effectively manage the development of alteration patina, offering a promising solution for mitigating ancient glass alteration while maintaining its aesthetic integrity.

1. Introduction

Although glass is often considered as durable and inert,[1] it is susceptible to deterioration, which can occur either immediately upon exposure to the atmosphere,[2] or gradually over extended periods. Several factors contribute to the initiation and progression of alteration phenomena,[3] highlighting the importance of developing effective methods to slow the ageing process and protect the glass surfaces. Such approaches not only enhance the durability of glass but also align with broader sustainability efforts by extending the lifespan of this versatile material.

Glass alteration occurs through corrosion processes, primarily driven by the reaction of the glass network with water.[4] Depending on atmospheric moisture conditions[5] (above or below saturation) and the specific glass composition,[6] various surface phenomena can appear.[3] Recent studies on silicate glass have revealed that natural degradation may result in the formation of opaque and heterogeneous alteration layers on the surface, arising not only from chemical transformations[7] but also from changes in the physical state of the glass surface.[8,9] These alteration layers form through concurrent mechanisms,[10] including the cyclic solubilization and reprecipitation of silica as corrosion-derived nanoparticles (c-NPs).[11] These c-NPs, along with other corrosion products, contribute to the development of compact patinas that significantly alter the glass' appearance, resulting in effects such as dulling,[12]

G. Franceschin, S. Centenaro, A. Traviglia
Center for Cultural Heritage Technologies (CCHT)
Istituto Italiano di Tecnologia (IIT)
Epsilon building, via Torino 155, Venezia-Mestre 30170, Italy
E-mail: giulia.franceschin@iit.it; arianna.traviglia@iit.it

The ORCID identification number(s) for the author(s) of this article can be found under https://doi.org/10.1002/admi.202500152

DOI: 10.1002/admi.202500152

S. Centenaro, E. Cattaruzza
Dipartimento di Scienze Molecolari e Nanosistemi (DSMN)
Università Ca' Foscari Venezia
Eta Building, via Torino 155, Venezia-Mestre 30170, Italy

M. Lorenzoni, R. Carzino, L. Ceseracciu
Materials Characterization Facility
Istituto Italiano di Tecnologia
via Morego 30, Genova 16163, Italy

S. Lauciello
Electron Microscopy Facility
Istituto Italiano di Tecnologia
via Morego 30, Genova 16163, Italy

iridescence, or sometimes more complex phenomena akin to photonic crystals.[13] While these patinas may act as partial barriers, reducing alkali ion leaching and slowing the breakdown of the silicate network,[8,14,15] they inadequate to prevent long-term and severe damage to the glass structure.

Traditionally, thermoplastic and thermosetting resins have been widely used for the repair and reinforcement of silicate glass. However, concerns about their toxicity and limited compatibility with glass substrates present significant challenges. To answer these issues, new formulations have been developed that not only functionally replace traditional polymeric materials but also offer enhanced substrate environmental compatibility.[16]

Room temperature sol-gel silica coatings have emerged as a promising alternative for the conservation of silicate glass.[16] Despite their potential, standard acid-catalyzed solutions pose risks to glass integrity,[3] particularly for lead-containing or heavily altered compositions.[17] Additionally, the necessity to maintain synthesis at near room temperature often leads to extended polymerization times, which can limit the practicality of such treatment for application.[18]

To address these challenges, this study explores the efficacy of sol-gel silica coatings synthesized under mild acidic conditions to prevent glass surface degradation. The primary objective is to create a fast-consolidating barrier on glass surfaces by utilizing silica glass fundamental components of glass itself. The focus is on developing coatings exclusively from nanostructured silica gel, designed not only to share a similar composition with the underlying material but also to replicate the structure naturally formed during glass degradation. This strategy seeks to minimize acidic conditions, reduce disparities in optical and chemical properties, and enhance both chemical stability and protective barrier performances.

Silica thin films, when applied to glass surfaces, have demonstrated a wide range of functionalities in various applications, including protection from water permeation,[19,20] atomic oxygen attack, and surface corrosion.[21,22] These films have synthesized using diverse routes and precursors,[23–26] with the sol-gel method being particularly favored for its versatility, homogeneity, low processing temperature and scalability.[27,28]

The sol-gel coating process involves applying a stable suspension of particles in a liquid (the *sol*) to a surface. Once applied, the solvent evaporates, leading to the formation of a *gel*. The resulting structure, more precisely described as a xerogel, undergoes further densification on the surface. A critical step in this process is curing, which finalizes the condensation and crosslinking of Si-O-Si chains from the active groups present in the *sol* particles. The rates of hydrolysis and condensation reaction in sol-gel processes can be significantly enhanced by either acidic or basic catalysts.[29] The choice of catalyst also determines the physicochemical properties of the final material. Under acidic conditions, the process favors the formation of highly polymerized silica networks, leading to the growth of interconnected silica chains. In contrast, basic conditions promote the rapid nucleation and growth of colloidal silica particles,[30] resulting in less cross-linked structures.[31,32] For glass coating applications, sol-gel formulations reported in literature often rely on highly acidic conditions (pH 1–2) to ensure the formation of transparent, dense and resistant films. This is primarily because alkaline corrosion of glass can lead to more aggressive and rapid degradation than acidic corrosion.[3,33] For this reason, basic conditions must be preferentially avoided in conservation treatments for historical and ancient glass. In contrast, acidic sol-gel formulations can be tailored to minimize glass corrosion while maintaining their protective function. This is typically achieved by incorporating acid or lead-based catalysts to improve film density and accelerate polymerization.[16,22] However, when these formulations are intended for cultural heritage or artistic objects, the challenge lies in balancing sufficient film density with minimal use of acid catalysts to prevent corrosion processes induced by the acidity. Acidic conditions, determined by the addition of catalytic molecules, directly affects the degree of polymerization of the sol-gel film after application. In some cases, thermal treatments are necessary to complete the polymerization process.

It is noteworthy that when ethyl alcohol is used as a solvent, hydrolysis -and, consequently film deposition- is negligible if the acid catalyst concentration falls below 0.003 M.[34] Beyond catalyst concentration, other factors can significantly improve the network densification of sol-gel coatings. These include the choice of silica precursor, the *sol* ageing time before deposition, the incorporation of pre-synthesized nanoparticles (NPs) into the formulation, and the precise control over film thickness, which is also influenced by the deposition technique employed.[35–39]

The coatings were designed to be fully inorganic to ensure high compositional compatibility with the glass substrate and long-term stability. Their properties were controlled by adjusting both the synthesis and surface deposition parameters, with the primary goal of producing films that would be largely imperceptible to the naked eye on the treated surfaces. To achieve this, different sol-gel solutions were obtained using a Stöber synthesis method, starting with tetra ethoxy silane (TEOS), water, ethanol (EtOH) and a minimal amount of hydrochloric acid (HCl) as a catalyst, with the concentration of HCl set to a lower limit of 0.003 M, as mentioned above, maintaining a pH between 4 and 4.5 throughout the synthesis process. TEOS was selected as silica precursor because it is a fully inorganic compound, and it could allow to obtain thin films with a composition as much as possible compatible with the silicate glass substrate composition. Colloidal suspensions of non-mesoporous silica NPs of 50 nm and 200 nm were incorporated into the sol-gel precursor formulation to assess their potential in improving the film's properties after densification and controlling the growth of corrosion products on the treated surface. The selection of non-mesoporous silica NPs was driven by the aim of creating a dense coating for surface protection and transparency. The presence of mesoporosity in the NPs would have introduced an additional variable to explore in the coating characterization. The choice of the NPs sizes was based both on their commercial availability and the uniformity achievable through synthesis for non-mesoporous silica NPs.[40,41] Additionally, the 200 nm NPs were selected as the upper size limit to ensure they remained below the visible light wavelength range, thereby minimizing optical interference in the sol-gel coatings. The 50 nm nanoparticles were selected because this is the smallest size at which non-porous silica nanoparticles can typically be synthesized with a uniform spherical shape and monodispersed size. Below this size, achieving such characteristics becomes increasingly challenging.[42]

All the formulations were applied on silica-lime glass slides via dip-coating, followed by characterization from structural,

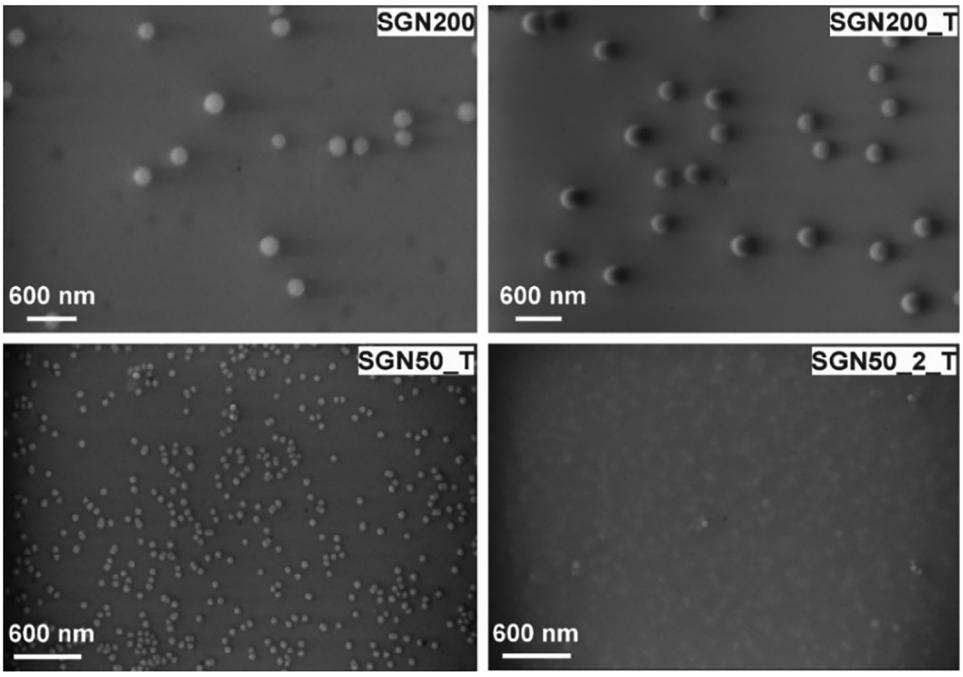

Figure 1. Characteristic morphology observed with SEM on the studied coatings SGN200, SGN200_T, SGN50_T and SGN50_2_T. In the double-layer coating SGN50_2_T a significant portion of the NPs appears to be covered by the sol-gel matrix, unlike in the single-layer coatings, where the NPs seem to be only partially incorporated into the matrix. Another aspect that can be observed is that the film obtained through a double dip-coating process exhibits the highest NPs surface concentration, which is logically related to the substrate undergoing two coating cycles.

morphological, optical, and mechanical perspectives. These properties were monitored both before and after an accelerated ageing process, designed to mimic natural environmental degradation. The multi-technique characterization approach encompassed atomic force microscopy (AFM), scanning electron microscopy (SEM), static contact angle, nanoindentation, and mechanical analyses.

This study lays the foundation for the use of silica coatings prepared through sol-gel synthesis under mild acidic conditions, offering a promising solution for the conservation of highly sensitive surfaces, such as those of ancient artifacts and works of art.

2. Results and Discussion

Before examining the coatings' resistance to corrosion and barrier properties, a comprehensive analysis of their physical, structural, optical and mechanical characteristics was conducted to assess the influence of coating parameters, including composition, deposition and densification. Preliminary adhesion tests, carried out to assess the effect of omitting surface activation treatments, showed no macroscopic changes in coating appearance and no signs of flaking or delamination.

2.1. Physical and Structural Properties of the Prepared Coatings

The thickness of the obtained films, determined using stylus profilometry, was measured to be between 95 and 108 nm. This measurement was taken from the pure sol-gel composition and is considered representative of the sol-gel matrix thickness in all composite coatings with a single layer. The uniformity of the coatings was influenced by the sol composition, the coating deposition parameters, and the film densification temperature. Detailed results of the analysis are available in the Table S3 of the Supporting Information. Notably, the homogeneity and integrity of the films were affected by the addition of NPs, with composite formulations containing NPs showing improved quality compared to pure sol-gel (SG) compositions, and for the films densified at 50 °C.

Chemically, all films consist of a pure silica sol-gel matrix embedding silica NPs of varying sizes. This composition was confirmed for all prepared samples through SEM-EDXS analysis. Detailed results regarding the chemical analysis of the films are available in the Supporting Information (Figure S1, Supporting Information). In addition to an enhanced homogeneity of the sol-gel matrix achieved through densification at 50 °C, the structure of the composite films was found to differ primarily in terms of NPs distribution and density. These variations are influenced by both the NPs sizes and the thickness of the sol-gel layers. **Figure 1** highlights the relationship between NPs size and their surface concentration in the final coating: at a constant volume concentration in the coating solutions, smaller NPs lead to a higher surface concentration in the final coatings. This effect of particle size on concentration and distribution is well-documented in the coating literature,[40,43] which shows that surface density is inversely proportional to the cube of the NPs diameter d_{NP}.

The NPs appears embedded within the silica sol-gel matrix, with no observable effect of the thermal treatment on their embedding depth. By combining AFM results with the known

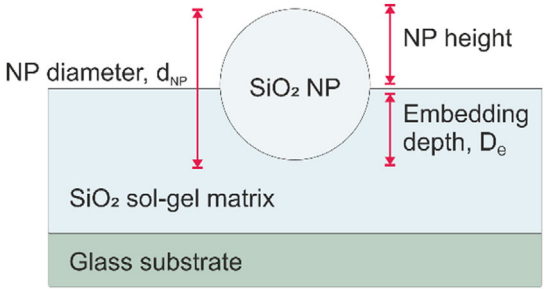

Figure 2. Schematic representation of the NPs embedded in the silica matrix. The representation is useful to understand the definition of embedding depth D_e.

average diameter of the NPs (d_{NP}) used in each film, the embedding depth (D_e) of the NPs was estimated. **Figure 2** illustrates the inferred nanoparticle inclusion scheme for both thermally treated and non-thermally treated samples, providing a visual clarification of the D_e concept.

As indicated in **Table 1**, the D_e values were found to be higher for films with NPs of 50 nm, where the D_e reached at least 80% of the d_{NP}. For 200 nm NPs, the least penetration depth was 30% of the d_{NP}. Based on these results, thermal energy appears to have slightly favored the embedding of the silica NPs in the composite films with 200 nm NPs and double-dip 50nm NPs, while it had no observable influence on the composite film with single-dip 50nm NPs (SGN50).

The use of NPs with regular spherical shapes is frequent in various research works of composite film preparations to modify surface wettability,[44] a property that strongly depends on the surface chemistry, structure, and roughness at the micro- and nanoscale. Differently from superhydrophobic sol-gel coatings, which are commonly obtained using hybrid organic-inorganic silica compositions,[45] the coatings prepared here are fully inorganic. As a result, their hydrophobicity is solely determined by structural and roughness characteristics only and is not expected to achieve superhydrophobicity. Water contact angle analysis performed on these coatings highlighted the influence of NPs size and thermal annealing on wetting properties. The results, reported in the (Figure S4 and Table S3, Supporting Information), indicated an increase in hydrophobicity for the pure sol-gel coatings that were thermally annealed (SG_T) compared to those that were not (SG). This increase in hydrophobicity was not observed or was less pronounced in all composite films embedding NPs.

The observed increase in both surface roughness and water contact angle for the thermally annealed sol-gel film is likely due to a higher densification rate induced by the thermal treatment, which may cause greater local disorder of the structure in comparison to the non-annealed film. In contrast, the surface roughness and wettability of the composite films appeared unaffected by the densification temperature. In this regard, the literature suggests that surface wettability is influenced by surface roughness, chemical composition, and surface energy,[46] as well as by surface distribution when heterogeneous phases are present, as in our case. The composite films did not show a direct correlation between measured roughness and hydrophobicity, likely due to their specific surface phase distribution and the possible influence of NPs in film densification.

Table 1. Values obtained from AFM analysis. The scanning area for each image was selected to maximize the information in relation to the average NPs size (d_{NP}). The range of the NPs height and the average NPs height values were determined considering a set of 8 random particle for each AFM image. The embedding depth D_e was calculated by subtracting the average NPs height from the d_{NP} value.

	Thermal treatment	Scanning area [µm × µm]	NPs diameter [nm]	Range NPs height [nm]	Average NPs height [nm]	NPs diameter [nm]	D_e [nm]
SGN200		10 × 10	200	130 – 152	140 ± 5	200	60 ± 5
SGN200_T	x	10 × 10	200	90 – 140	104 ± 5	200	96 ± 5
SGN50		5 × 5	50	9 – 13	10 ± 2	50	40 ± 2
SGN50_T	x	5 × 5	50	9 – 14	11 ± 2	50	39 ± 2
SGN50_2		5 × 5	50	2 – 9	7 ± 2	50	43 ± 2
SGN50_2_T	x	5 × 5	50	1.5 – 8.5	4.5 ± 2	50	45 ± 5

Additionally, it is important to note that the areas used to calculate surface roughness are significantly smaller than those used for water contact angle measurements. Specifically, the diameter of the water drop is 3 mm, while the AFM scanning area ranges from 5 to 10 µm. This difference in measurement scales may have hindered any direct relationship between surface roughness and wettability properties.

To evaluate the optical properties and ensure that the coatings maintain the original surface appearance, reflectance analysis was performed on the selected films. The total reflectance spectra – reported in Figure S2 of the Supporting Information – show no absorbance peak in the visible range for any of the films, except for one broad absorption band in the double-dip sample. Specifically, this film presents a broad band between 425 nm and 700 nm, with a maximum of 8% total reflectance at 550 nm, which is close to the values measured for untreated glass. The total reflectance of the other coated samples is on average, 1–2% lower than that of the uncoated samples in the whole visible range (Figure S3, Supporting Information). In addition, the diffuse reflectance spectra (Figure S2, Supporting Information-right) show higher values in the samples prepared with 200 nm NPs, consistent with the higher surface roughness observed in the AFM analysis of these samples. Conversely, the coatings embedding 50 nm NPs and the pure sol-gel coatings have diffused reflectance comparable to that of untreated glass, which also aligns with the reported values of surface roughness. In any case, the maximum values of both diffuse and total reflectance differ from the values of uncoated glass of values that are below the threshold required for optical perception by the naked eye.

2.2. A comparison of the Ageing Resistance in the Different Formulations

The analysis of the samples after ageing provided a clear assessment of the protective properties of each formulation against glass corrosion. Upon initial observation, the coated areas in all samples treated with the NPs-charged compositions appeared visibly clearer and less altered compared to both the untreated areas and those treated with the pure SG composition. Optical microscopy, as shown in Figure 4a, confirms this finding by revealing the absence of bright spots—indicative of early-stage corrosion products—in the treated areas, unlike in the untreated regions. These bright spots signal the initial formation of the glass corrosion patina in the uncoated glass. In the area covered by the coating, the nuclei of forming corrosion products are extremely small or nearly absent in the sample coated with the double layer of film. Subtle variations in opacification among the coated areas with different formulations were discernible only under higher magnification. **Figure** 3b–f further illustrate these differences, with the double dip-coated sample displaying significantly fewer bright spots, underscoring its enhanced resistance to alteration during aging.

Aggregation of chemical elements were systematically detected using SEM-EDS on the surface of uncoated glass (**Figure** 4), suggesting that ageing induced corrosion products such as Na and Ca salts, in addition to aggregation of c-NPs. In contrast, on the coated samples no salts were detected but only aggregated silica c-NPs derived from the corrosion process, suggesting a degree of protection produced by the application of the coating.

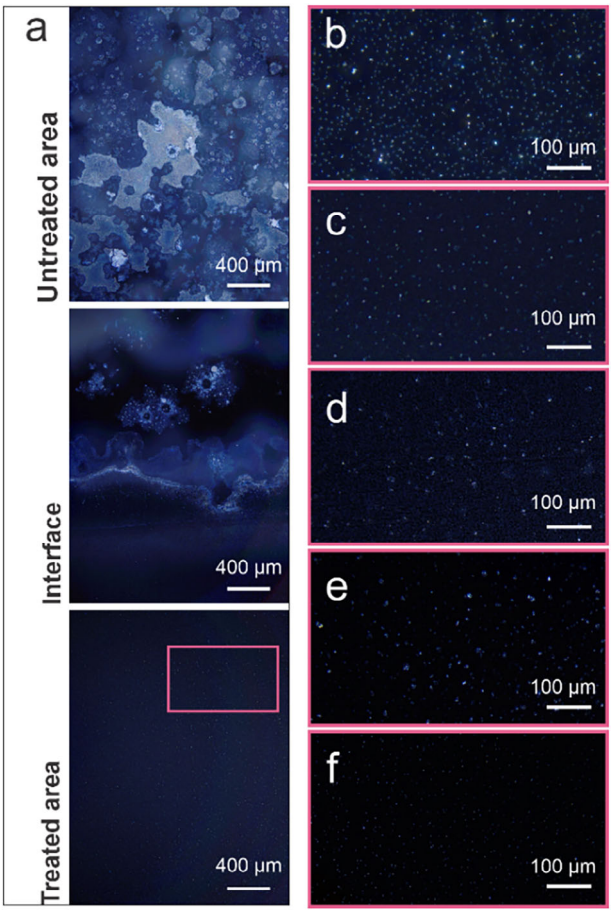

Figure 3. a) Optical microscope images collected at 5x magnification for SGN200 coating, showing the untreated area (top), the interface between treated and non-treated areas (middle), and the treated area (bottom). Images captured at 40x magnification and fixed brightness for b) SG, c) SGN200, d) SGN200_T, e) SGN50_T and f) SGN50_2_T.

SEM imaging highlighted also peculiar structural differences developed after ageing in the coatings, as reported in Figure 4d–g. Interestingly, the addition of SiO_2 NPs in the single-layer coatings appeared to exert a templating effect on the formation and growth of c-NPs, limited to the areas surrounding the added NPs. Compared to the coating morphology before ageing in Figure 1, the most significant alterations were observed in the non-thermally annealed composite coating with 200 nm NPs, whereas the least changes occurred in the formulation with 50 nm NPs and a double-layer design (SGN50_2_T). In all coated samples, unlike the uncoated ones, SEM-EDS analysis demonstrated that the surface remains chemically homogeneous compared to the composition observed before ageing. Even in regions with altered structures, such as those circled in red in Figure 4, all elements are homogeneously distributed in the EDS chemical maps. This confirms that no corrosion products other than c-NPs were formed after ageing. In Figure 4d, no regions are highlighted in red, as it was not possible to identify structural differences in the

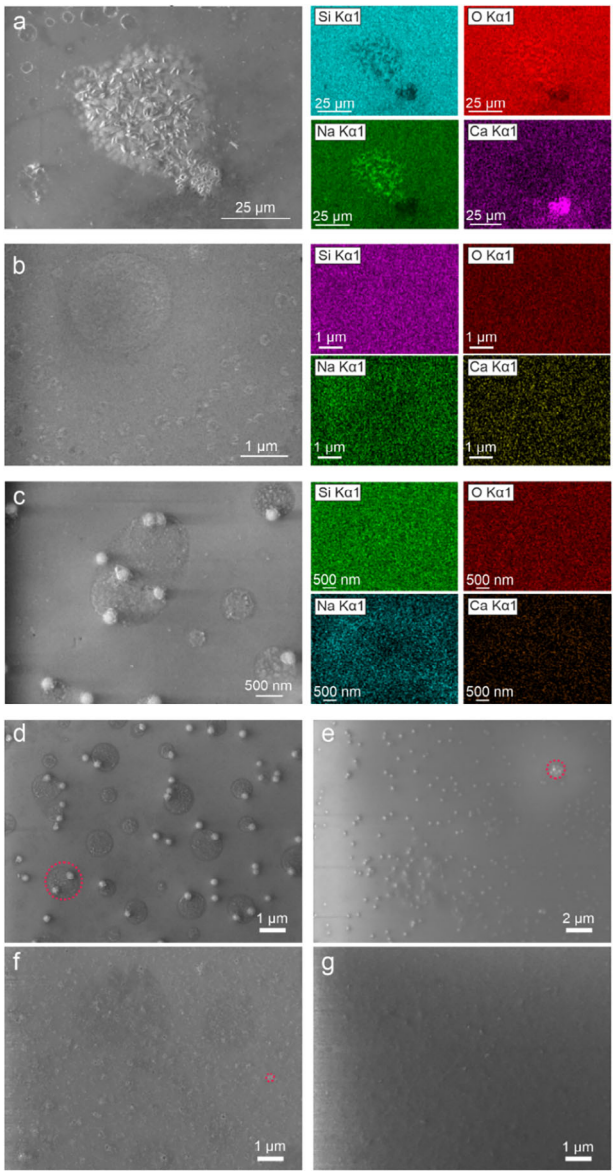

Figure 4. SEM-EDS mapping of typical alteration structures observed after ageing on a) uncoated glass, b) SG and c) on SGN200 sample. SEM images of the coatings post-ageing allow for the evaluation of structural evolution differences across the different compositions: d) SGN200, e) SGN200_T, f) SGN50_T, g) SGN50_2_T. In (d), (e) and (f), the regions highlighted in red indicate areas of silica nanoparticle aggregations formed after ageing the samples. Na and Ca aggregations were observed only in the uncoated glass (a), while a homogenous distribution of Si, O, Na, and Ca was consistently detected in the coated glass (b) and (c), even in areas where the granular alteration structures appeared after ageing.

double-dip coated sample before and after ageing due to the limited size of the altered spots.

This effect was further confirmed by AFM analysis. **Figure 5** shows that unprotected glass surfaces exhibited corrosion structures characterised by randomly distributed aggregates of silica NPs, like those shown by SEM analysis. In contrast, glass samples coated with a sol-gel layer containing silica NPs, regardless of their size (200 nm or 50 nm), exhibited distinct development of silica c-NPs aggregates proximal to the added NPs, suggesting their role as preferential sites for alteration patina formation. Notably, these formations displayed regular circular geometries surrounding individual NPs, with dimensions correlating to the initial NP size.

The values of surface roughness measured with AFM analysis on the aged samples are shown in Table S4 (Supporting Information). Remarkably, in samples treated with a double-layer coating, the roughness and size of the NPs remain unaltered before and after the ageing treatment, indicating the efficacy of the dual immersion coating in impeding corrosion progression. Conversely, a single layer of coating was found to fail in preventing corrosion initiation, albeit mitigating macroscopic patina effects compared to untreated glass surfaces.

Linking surface properties with the water contact angle analysis, it is interesting to examine the difference between the measured contact angles before and after sample ageing, as reported in **Table 2**. Even if *CA* value apparently increased after ageing, their interpretation must consider the nature of the surfaces being analyzed, which are characterized by heterogeneously distributed rough textures. For such surfaces, varying effects on the water contact angle can occur, as explained by the Cassie-Baxter[47] and Wenzel models.[48] However, in this study, the droplet size used in the contact angle measurement may be comparable to the underlying surface pattern. Under these conditions, the droplet size may not be large enough relative to the surface patterns, making it impossible to draw definitive conclusions about the relationship between the water contact angle and surface structure using the aforementioned models.[49]

Nevertheless, it is worth considering the difference of standard deviation values of each measurement (*std dev* in Table 2), which are notably higher for the films after ageing and show a minimum for the films obtained with a double-dip deposition. Since standard deviation reflects the consistency of the five measurements taken for each sample to obtain the average contact angle, it provides insight into the homogeneity of the surface roughness in the analyzed area. After ageing, the lower standard deviation in the double-dip coating system suggests that this coating maintained a more homogeneous surface roughness compared to the other formulations, particularly the pure sol-gel one, which exhibited the highest variation in both *CA* and *std dev*. This indicates that it was likely less altered by the ageing process than the coatings obtained with a single dip, as also indicated by AFM results.

The highest coating resistance and lowest roughness observed in the double-dipped sample were further supported by diffuse reflectivity data, which account for backscattering effects due to surface roughness. The difference in diffuse reflectivity $\Delta R_{diffuse}$ between the spectra after and before ageing is expected to increase as the coating becomes rougher after ageing. Unprotected glass indeed showed the formation of corrosion products on the surface after ageing, leading to a degradation of surface flatness. Therefore, in general, a higher $\Delta R_{diffuse}$ value indicates that the coating is less effective in protecting against alteration.

As shown in **Figure 6** (left), the $\Delta R_{diffuse,AGED}$ pattern is significantly higher for the uncoated glass and decreases for the coated samples, indicating that ageing induces the formation of a rougher surface in the uncoated glass. Additionally, differences in the behaviors of the studied coating compositions are evident,

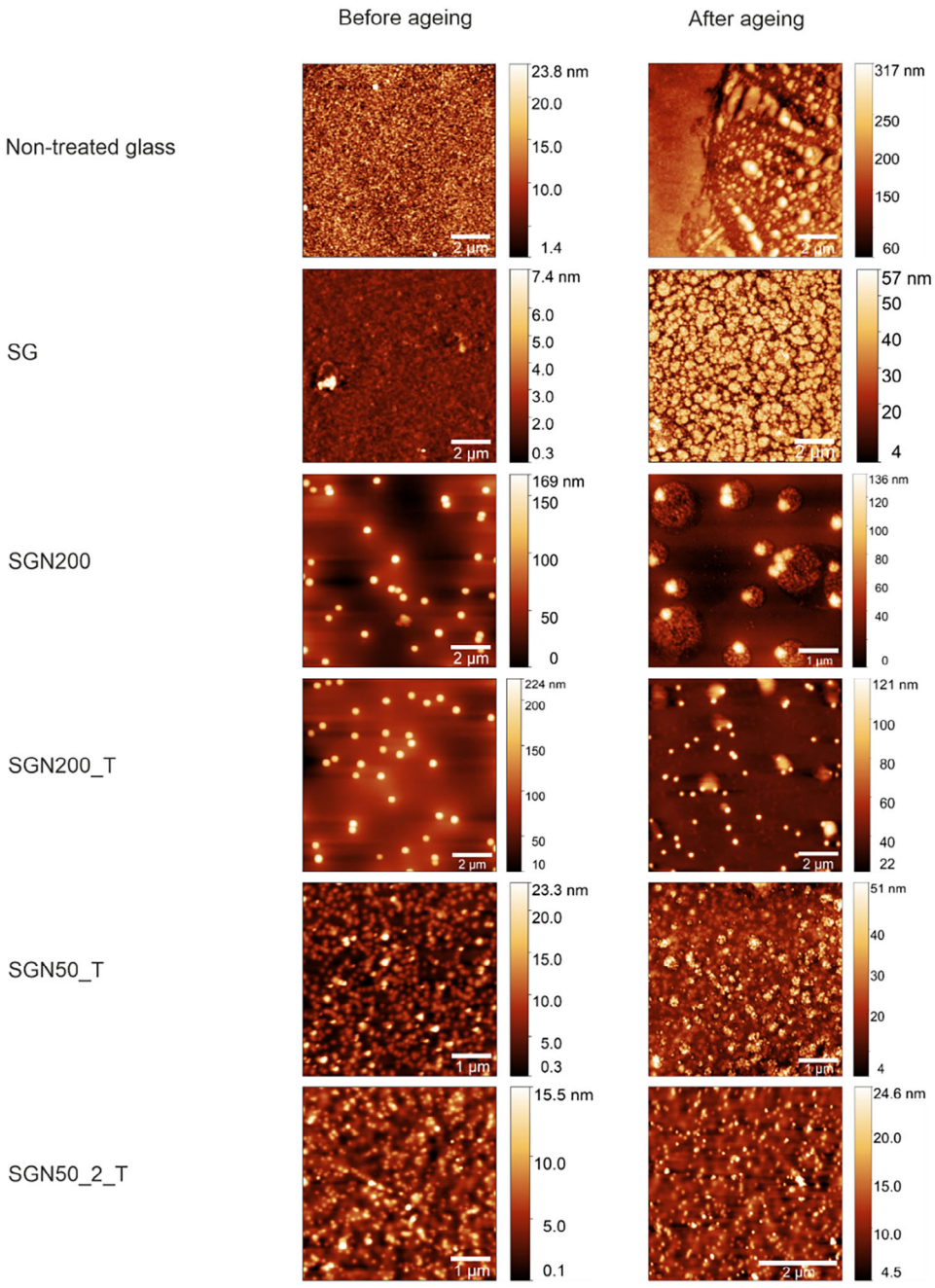

Figure 5. AFM images of the sample surfaces before and after ageing. The color scale for each image is optimized to enhance contrast and highlight surface features.

Table 2. Water contact angle (CA) values with the relative standard deviation measured for each studied sample before and after ageing process.

	CA_{in}	std dev_{in}	CA_{aged}	std dev_{aged}
SG	20.1	0.3	72.0	3.1
SGN200	20.1	0.2	71.8	15.6
SGN200_T	36.0	0.3	54.5	14.4
SGN50_T	34.7	0.4	89.4	4.9
SGN50_2_T	40.1	2.7	80.0	9.3

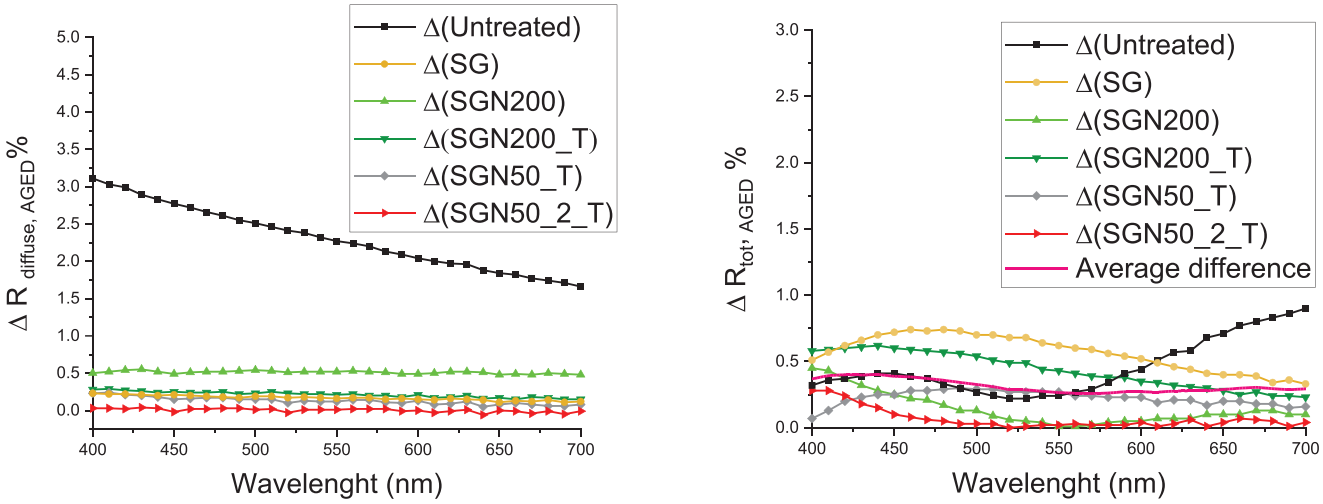

Figure 6. Differential patterns calculated between the diffuse reflectance % $R_{diffuse}$ (left) and the total reflectance % R_{tot} (right) of the samples respectively after and before the ageing process. The total reflectance spectra of the aged samples are available in the (Figure S5, Supporting Information).

with the double-dipped glass exhibiting a $\Delta R_{diffuse,AGED}$ trend that approaches zero. This suggests that the diffuse reflectance of the double-dip coating remains nearly stable after ageing. In other words, no visible alteration in surface roughness is detected for this sample, unlike the other compositions, which all show an increase in $R_{diffuse}$ after ageing, despite the thermal treatment having a beneficial effect on coating stability (lower $\Delta R_{diffuse,AGED}$ values). The $\Delta R_{tot,AGED}$ in Figure 6 (right) displays an average value around 0.3, which indicated that no remarkable differences of the total reflectance were developed after ageing. The highest increase in total reflectance was recorded for the pure sol-gel film between 400 and 600 nm, and for the untreated glass above 600 nm.

Interestingly, the increase in the backscattering ratio in single-layer coatings, compared to the double-layer coatings, is perfectly consistent with the surface roughness measurements obtained by AFM and SEM-EDS analysis after ageing.

The structural compatibility of the studied coatings with glass substrates was confirmed by mechanical analysis using nanoindentation measurements. The resulting dynamic curves and their detailed analysis are presented in Figure S6 of the Supporting Information and indicate that the elastic modulus (E) and the hardness (H) of all coating films approach but do not exceed those of the pristine glass slides. The most significant decrease in E and H is observed in the double-dip-coated sample, which suggests that the lower values of all coatings are realistic and do not arise only from low-depth artefacts. After ageing, both E and H tend to increase, approaching the values typical of bulk glass, implying that the coating are becoming harder and more rigid under extreme conditions. Although E modulus showed only slight increases, particularly in the composite coating non thermally treated and the pure sol-gel one, no significant changes were observed in the other samples. However, a clear increase in average H values was noted in almost all samples, except for those treated with a double layer and those heat-treated with 200 nm nanoparticles. The sample prepared with a double coating exhibited the smallest variation in the average values of both E and H, which remained lower than those of all other samples, even after the ageing process.

2.3. Comparison with Existing Sol-Gel Coatings

Several studies have explored hybrid organic-inorganic sol-gel coatings for corrosion protection on metals, where the incorporation of organic components into the silica network has been shown to enhance durability and barrier properties. For example, organic groups in silica sol-gel coatings have been demonstrated to improve their performance under harsh environments by reducing porosity and enhancing mechanical stability.[50–52]

The current work diverges from this corrosion-focused research by evaluating the environmental stability of fully inorganic silica coatings, specifically designed for cultural heritage glass substrates. For such applications, the primary concern is not corrosion but rather surface repair, long-term transparency, and stability against environmental degradation. Unlike hybrid sol-gel coatings optimized for corrosion protection in metals,[53,54] the coatings examined here are intended for transparent applications, where maintaining optical properties (such as transparency retention and surface integrity) is crucial. Therefore, traditional electrochemical corrosion resistance tests are less relevant to the goals of this study, which prioritizes durability under environmental stressors like humidity and thermal cycling.

Corrosion resistance of coatings is often assessed using electrochemical techniques like electrochemical impedance spectroscopy (EIS) and Tafel analysis,[55] which are well-suited for conductive materials, like metals.[56] However, since glass is an insulating material, it does not support direct electrochemical measurements. This inherent limitation, along with the need for a conductive substrate or specific modifications (e.g. conductive coatings), made these methods unsuitable for the present investigation, where the primary concern is not corrosion but rather the long-term transparency and resistance to environmental degradation.

To the best of the authors' knowledge, there is no direct equivalent in the literature for the approach taken here – specifically, the use of silica films combined with silica nanoparticles to create transparent and durable coatings for cultural heritage glass. While previous studies have explored the incorporation of silica nanoparticles into sol-gel coatings, these typically focus on enhancing mechanical and thermal properties for corrosion protection in metal applications.[57,58] The addition of silica nanoparticles to sol-gel films has been shown to improve hardness, scratch resistance, and adhesion, but these works generally do not address the application of silica nanoparticle-based coatings on glass, nor their environmental stability in terms of transparency retention and resistance to ageing.

In contrast, the present research focuses on the long-term environmental performance of fully inorganic silica-based coatings, designed not only to provide mechanical protection but also to maintain optical properties when exposed to accelerated ageing conditions. The results show that these coatings exhibit minimal loss of transparency and surface integrity after exposure to environmental stressors, highlighting their potential for transparent applications. This represents a significant departure from traditional corrosion-focused studies, as it emphasizes maintaining the coatings' clarity and surface quality over time, rather than solely preventing corrosion.

The unique combination of silica films and silica NPs used in this research allows for the creation of a highly stable, fully inorganic network, which is uncommon in the literature for glass coatings.[16] Previous research has primarily focused on sol-gel coatings with organic-inorganic hybrid systems[59–61] or fully inorganic systems without embedded nanoparticles.[62–65] The current work fills this gap by demonstrating the feasibility of silica-based coatings for applications where optical clarity and environmental stability are critical. Additionally, it contributes to a deeper understanding of the structural modifications induces by NPs incorporation during ageing. Although no direct comparison with traditional highly acidic sol-gel formulations (pH ≈1–2) was performed in this study, the mildly acidic conditions adopted (pH ≈4) were expected to significantly reduce corrosive effects on silicate glass substrates, as supported by literature.[3,29,63,66,67] Throughout the coating and ageing processes, no visible or measurable signs of substrate degradation—such as etching, clouding, or surface roughening—were observed, suggesting enhanced compatibility of the developed formulation with sensitive glass surfaces.

It is worth noting that no specific surface pre-treatment was applied to enhance adhesion between the coating and the substrate; nevertheless, the coatings demonstrated strong adherence to the glass throughout the study. Preliminary adhesion checks, including washing tests with ethanol and water on samples prior to ageing, revealed no macroscopic delamination or changes in coating appearance. After ageing, no flaking or detachment was observed, and as shown in the SEM, AFM, and mechanical results, the coatings remained dense and compact on the glass surface. Although a systematic quantitative adhesion analysis was not included in this study, these combined observations indirectly support the reliability of the coating's adhesion. Furthermore, nanoindentation tests provided additional insight into adhesion behavior: no cracks, delamination, or defects were observed around the indents, even after ageing, as shown in Figure S7 (Supporting Information). While dedicated adhesion tests would be valuable to explore in the future, they were beyond the scope of this study. The overall stability of the coatings—supported by surface, mechanical, and morphological analyses—provides indirect but convincing evidence of their reliable adhesion and long-term durability, reinforcing their practical applicability for cultural heritage conservation and ensuring minimal intervention on fragile substrates.

3. Conclusion

Glass surfaces are vulnerable to environmental corrosion, which compromises both their functionality and their aesthetic appearance. This study demonstrated how composite silica-based coatings enhanced with silica NPs can provide an innovative solution to improve the anticorrosion performance of glass surfaces, combining durability with optical and mechanical integrity. Key factors, including the incorporation of NPs, their size, the temperature of film densification, and the number of dip-coating cycles, were systematically analyzed to assess their impact on the structure and properties of the deposited films.

The analyses confirmed that incorporating silica NPs significantly enhanced the performance of sol-gel coatings, an aspect particularly relevant when minimal acidity is required during application. The composite formulations demonstrated superior resistance to environmental corrosion, with optimal performances observed in the double-layer coating incorporating 50 nm NPs. These coatings effectively retained surface properties, reduced silica dissolution, and prevented the formation of corrosion products such as alkaline salts. In contrast, pure sol-gel coatings, while moderately effective at slowing surface corrosion, showed limitations in preventing silica precipitation and morphological changes after ageing.

The findings of this research also emphasize the crucial impact of NPs size and thermal annealing on the properties of the coating. Films incorporating 50 nm NPs exhibited enhanced hydrophobicity and corrosion resistance compared to those with 200 nm NPs, while thermally annealed coatings showed superior structural stability and barrier performance. These results highlight the importance of optimizing formulation and processing conditions to achieve greater film stability and protective efficacy.

Notably, the inclusion of NPs induced a templating effect on the morphology of silica aggregates formed during ageing. In particular, the silica NPs dispersions guided the formation of granular silica structures in the limited spaces surrounding the NPs after film ageing. The extent of these aggregates was directly influenced by the size of the incorporated NPs, underscoring the role of NPs dimension in determining coating performance.

This work advances our understanding of composite silica formulations incorporating silica NPs in protecting glass from atmospheric corrosion. The ability of these coatings to maintain both transparency and structural integrity highlights their potential as an effective solution for preserving glass in diverse environments. Beyond glass preservation, the broader implications of this research – including applications in heritage conservation and material repair – position composite silica coatings as a versatile and promising approach for addressing challenges in material protection and restoration.

4. Experimental Section

Materials: TEOS ($Si(OCH_2CH_3)_4$, 99% purity) and absolute EtOH (CH_3CH_2OH, 99,8% purity) were purchased by Merck and used without further purification. Ultrapure water was obtained with a Sartorius Arium® Pro purification system. Colloidal dispersions of silica NPs in water were purchased from nanoComposix (Non-functionalised NanoXact™ silica NPs of 50 nm and 200 nm) and used in the composite coating formulations with no further modification.

Commercial silica-soda-lime glass slides for microscopy observations, supplied by VWR, were employed as substrates for the coating depositions. They were cleaned by sequential immersion in soapy deionized water, ultrapure water, ethanol, and isopropanol for 10 minutes in a sonic bath. The cleaned slides were then air-dried and stored in a closed container until the coating deposition.

Sol Preparation by Stöber Method: The sol precursor was prepared by mixing ultrapure H_2O and EtOH for 10 min before adding TEOS dropwise, and HCl. This starting solution was prepared using a molar ratio of TEOS:EtOH:H_2O of 1:12:20 and an HCl concentration of 0,007 M, resulting in an initial pH of approximately 4. This pH value corresponds to that proposed by Watkins et al.[35] to minimize delamination effects on the films and was higher than the lower limit of 0.003 M, which was defined by Aelion et al. as ineffective for silica film formation.[34]

The sol was mixed at room temperature for 1 h before being applied to the substrates. This sol was used to prepare the pure sol-gel coating sample (Sol1 in Table S1, Supporting Information).

Silica Nanoparticles Addition to the Sol-Gel Mixture: A second set of sols (Sol2 and Sol3 in Table S1, Supporting Information) was obtained by adding colloidal suspensions of silica NPs to the previously described sol formulation. Two different sizes of silica NPs (50 nm and 200 nm) were used to prepare two different sols containing a total concentration of 1 mg ml^{-1} of silica NPs. The molar ratio of TEOS:EtOH:H_2O was kept at 1:12:20.

The NPs in water suspension were first diluted in ultrapure H_2O to the desired concentration and mixed with EtOH for 10 min before adding TEOS and HCl. The initial pH of the silica NPs suspensions used in the syntheses was found between 7 and 7.5, in line with the supplier's specifications. Upon incorporation into the HCl-catalyzed sol, the pH of the final formulation was effectively adjusted to ≈4, ensuring compatibility with the mildly acidic synthesis conditions used in this study.

All the different sols were mixed for 1 h at room temperature before being applied as a coating.

Coating Deposition and Film Densification: Before deposition, the glass slides were cleaned and air-dried according to the protocol described in the Materials section. No additional pre-treatment was applied to enhance coating adhesion, as the process relied on the inherent chemical compatibility between the silica substrate and the sol-gel precursors to ensure sufficient adherence.

All the films were deposited on glass slides using a dip-coating deposition system (ND-DC, Nadetech Innovation, Spain). The coating was then densified using two different methods for each composition: one by maintaining the coating at room temperature, and the other by subjecting it to a mild thermal treatment at 50 °C for 45 hours. The temperature of 50 °C was selected based on practical considerations: it was sufficiently above ambient temperature to promote effective densification yet remains below 60 °C to avoid potential degradation of residual organic materials that may be present on archaeological glass substrates. This careful balance was intended to ensure the treatment would be safe and practical for application on ancient and fragile glass objects.

The immersion rate, withdrawal rate and immersion time were kept constants for all samples. The starting sol, the number of dips and the temperature during film densification varied within the sample set. The parameters used to obtain each coating sample were detailed in Table S2 (Supporting Information).

The coated slides, both those kept at room temperature and those subjected to thermal treatment, were held vertically immediately after the dipping process and throughout the densification phase. The samples densified with mild temperature treatment were maintained at 50 °C for 45 hours.

As no surface pre-treatment was applied to enhance adhesion between the coating and the substrate, preliminary adhesion tests were performed after densification by sonicating duplicate samples in ethanol and water for 10 minutes.

Accelerated Ageing of the Treated Glass Samples: After the deposition and densification processes, the films were aged in a climatic chamber under controlled humidity and temperature conditions designed to accelerate atmospheric ageing. The temperature was maintained constantly at 70 °C, while the relative humidity (RH) was cycled every 2 days between 10% and 90%. This ageing protocol continued for 3 weeks, beginning one month after the preparation of the coatings, to ensure complete densification of the sol-gel matrix.

Characterization Techniques: *Optical Microscopy Imaging*: Optical images were acquired using an Olympus BX43 optical microscope coupled with a 3.1-megapixel digital color camera (Olympus LC30). Image acquisition was realized in reflected darkfield mode with the CellSens Entry software. The sample was illuminated with a pE-300 white CoolLED fluorescence system enabling individual control of three excitation channels in the violet, blue and green regions to simulate white light.

Scanning Electron Microscopy: The SEM analysis was performed using a Zeiss GeminiSEM 560 (Zeiss, Oberkochen, Germany) field-emission gun, operating at an acceleration voltage of 5 kV. Since the samples were non-conductive and coating was not feasible, the Low-Vacuum mode was employed, operating at 120 Pa. Energy-dispersive spectroscopy (EDS, Oxford Instruments, X-Max, 80 mm^2), operating at 10 kV, was used to evaluate the presence and distribution of elements.

Thickness Evaluation: The thickness of the coating was measured using a mechanical, stylus-based surface profiler (KLA-Tencor AlphaStep 500). At least 3 line-scans were performed at different positions to obtain a representative thickness range. To prevent any potential damage or scratches to the coating, a stylus force of less than 7 mg was applied.

To evaluate the surface properties of the coatings before ageing and the effect of the densification treatment on the NPs embedding, AFM analysis was performed on all films both thermally treated and non-thermally treated.

AFM measurements were performed in non-contact mode with an XE-100 by Park Systems, in air at room temperature (RH < 35%). During scan the AFM was mounting commercial probes (AC160TS). Raw data were processed with Gwyddion software, providing surface roughness, most typically root mean square value of irregularities (RMS).

Diffuse and Total Reflection Analysis: Diffuse and total reflection spectra were collected using a portable Konica Minolta CM 700d spectrophotometer. The instrument features a pulsed xenon light source that diffusely illuminates the sample, and a silicon photodiode that detects the light at an 8° angle from the normal line. For diffuse reflectance analysis, spectra were acquired excluding the specular component, while for total reflectance analysis, the specular component was included. Both types of spectra were measured within a 400 – 700 nm wavelength range. To avoid boundary effects, the illuminated circular area was positioned at the center of each sample, using a 3 mm aperture. Each sample was analyzed before and after the ageing process by averaging 2 measurements taken at a single point of analysis to calculate the average spectrum for each sample.

Water Contact Angle Analysis: Wettability measurements were performed with the sessile drop method using a DataPhysics OCAH 200 contact angle goniometer under laboratory conditions (temperature 22–25 °C and relative humidity 50–60%). For the characterization, droplets of 5 µl volume MilliQ water were used. For each sample 5 measurements were performed in 5 different points and used to calculate an average value.

Nanoindentation and Mechanical Testing: The mechanical properties of all samples were characterized by Nanoindentation on an Anton Paar UHNT nanoindenter equipped with a pyramidal Berkovich tip. To address the testing challenges posed by the low thickness and its variation among samples, dynamic indentation was employed. This technique involves applying a small amplitude oscillation during the conventional indentation routine, allowing the mechanical properties to be extracted at each cycle and providing a profile of mechanical properties as a function of

indentation depth. The maximum load reached during indentations was 50 mN, with a loading rate of 10 mN min^{-1}, dwell time of 20 s and unloading rate 50 mN min^{-1}. The oscillation amplitude was progressively increased up to 0.5 mN min^{-1}, with 5 Hz frequency. From each test, plots of Elastic modulus E and hardness H as a function of the indentation depth were obtained.

Supporting Information

Supporting Information is available from the Wiley Online Library or from the author.

Acknowledgements

This work was partially funded by the European Union's Horizon Europe research and innovation action under the grant agreement No. 101060768 (GoGreen project).

Conflict of Interest

The authors declare no conflict of interest.

Data Availability Statement

The data that support the findings of this study are openly available in Repository at https://doi.org/10.48557/GIDEMZ, reference number 48557.

Keywords

antifouling glass coatings, composite thin films, dip-coating, silica nanoparticles, sol-gel silica

Received: February 18, 2025
Revised: May 9, 2025
Published online: May 22, 2025

[1] T. Chinni, A. Silvestri, S. Fiorentino, M. Vandini, *Heritage* **2023**, *6*, 662.
[2] A. M. Filbert, M. L Hair, in *Advances in Corrosion Science and Technology*, (Eds. M. G. Fontana, R.W. Staehle), Springer, US **1976**, *5*, 1–54
[3] R. Zanini, G. Franceschin, E. Cattaruzza, A. Traviglia, *npj Mater. Degrad.* **2023**, *7*, 1.
[4] A. Tournié, P. Ricciardi, P. Colomban, *Solid State Ionics* **2008**, *179*, 2142.
[5] F. Alloteau, O. Majérus, I. Biron, P. Lehuédé, D. Caurant, T. Charpentier, A. Seyeux, *Corros. Sci.* **2019**, *159*, 108129.
[6] F. Alloteau, O. Majérus, V. Valbi, I. Biron, P. Lehuédé, D. Caurant, T. Charpentier, A. Seyeux, *npj Mater Degrad* **2020**, *4*, 1.
[7] R. Zanini, G. Franceschin, E. Cattaruzza, M. Prato, M. Barozzi, A. Traviglia, *J. Non-Cryst. Solids* **2023**, *612*, 122356.
[8] O. Schalm, W. Anaf, *J. Non-Cryst. Solids* **2016**, *442*, 1.
[9] M. I. Ojovan, *MRS Adv.* **2020**, *5*, 111.
[10] G. Franceschin, R. Zanini, G. Iori, E. Longo, G. Divitini, G. Tromba, A. Traviglia, *Phys. Chem. Chem. Phys.* **2024**, *26*, 9697.
[11] S. Gin, X. Guo, J.-M. Delaye, F. Angeli, K. Damodaran, V. Testud, J. Du, S. Kerisit, S. H. Kim, *npj Mater Degrad.* **2020**, *4*, 1.
[12] O. Schalm, G. Nuyts, K. Janssens, *J. Non-Cryst. Solids* **2021**, *569*, 120984.
[13] G. Guidetti, R. Zanini, G. Franceschin, M. Moglianetti, T. Kim, N. Cohan, L. Chan, J. Treadgold, A. Traviglia, F. G. Omenetto, *Proc. Natl. Acad. Sci. USA* **2023**, *120*, 2311583120.
[14] C. Lenting, O. Plümper, M. Kilburn, P. Guagliardo, M. Klinkenberg, T. Geisler, *npj Mater. Degrad.* **2018**, *2*, 1.
[15] S. Gin, P. Jollivet, M. Fournier, F. Angeli, P. Frugier, T. Charpentier, *Nat. Commun.* **2015**, *6*, 6360.
[16] S. Centenaro, G. Franceschin, E. Cattaruzza, A. Traviglia, *J. Cult. Herit.* **2023**, *64*, 132.
[17] R. Bertoncello, L. Milanese, J. C. Dran, A. Bouquillon, *J. Non-Cryst. Solids* **2006**, *352*, 315.
[18] R. Bertoncello, L. Milanese, R. Negro, L. Saragoni, *J. Non-Cryst. Solids* **2003**, *324*, 73.
[19] A. Morlier, S. Cros, J.-P. Garandet, N. Alberola, *Thin Solid Films* **2012**, *524*, 62.
[20] L. Hu, M. Li, C. Xu, Y. Luo, *Thin Solid Films* **2011**, *520*, 1063.
[21] G. P. Thim, M. A. S. Oliveira, E. D. A. Oliveira, *J. Non-Cryst. Solids* **2000**, *273*, 124.
[22] D. Bianco, B. Bertoncello, *Nucl. Instrum. Meth. Phys. Res. Sec. B: Beam Interact. Mater. Atoms* **2008**, *266*, 2358.
[23] N. Nishiyama, S. Tanaka, Y. Egashira, Y. Oku, K Ueyama, *Chem. Mater.* **2003**, *15*, 1006.
[24] A. Walcarius, E. Sibottier, M. Etienne, J. Ghanbaja, *Nat. Mater.* **2007**, *6*, 602.
[25] A. Bearzotti, J. M. Bertolo, P. Innocenzi, P. Falcaro, E. Traversa, *J. Eur. Ceram. Soc.* **2004**, *24*, 1969.
[26] H. Okudera, A. Hozumi, *Thin Solid Films* **2003**, *434*, 62.
[27] C. J. Brinker, A. J. Hurd, G. C. Frye, P. R. Schunk, C. S. Ashley, *J. Ceram. Soc. Jpn.* **1991**, *99*, 862.
[28] D. B. Emrie, *J. Nanomater.* **2024**, *2024*, 6109770.
[29] C. J. Brinker, G. W. Scherer in *Sol-Gel Science: The Physics and Chemistry of Sol-Gel Processing*, Elsevier Inc., Amsterdam, Netherlands **2013**
[30] W. Stöber, A. Fink, E. Bohn, *J. Colloid Interface Sci.* **1968**, *26*, 62.
[31] T. Montheil, C. Echalier, J. Martinez, G. Subra, A Mehdi, *J. Mater. Chem. B* **2018**, *6*, 3434.
[32] Y. Lu, Y. Yin, B. T. Mayers, Y Xia, *Nano Lett.* **2002**, *2*, 183.
[33] S. Gin, P. Jollivet, M. Fournier, C. Berthon, Z. Wang, A. Mitroshkov, Z. Zhu, J. V. Ryan, *Geochim. Cosmochim. Acta* **2015**, *151*, 68.
[34] R. Aelion, A. Loebel, F Eirich, *J. Am. Chem. Soc.* **1950**, *72*, 5705.
[35] E. Watkins, C. Griffiths, C. Batchelor, P. Barker, M. Carnie, *Coatings* **2023**, *13*, 982.
[36] H. Kozuka, T. Michihata, H. Uchiyama, *J. Ceram. Soc. Jpn.* **2011**, *119*, 434.
[37] R. V. Lakshmi, P. Bera, C. Anandan, B. J. Basu, *Appl. Surf. Sci.* **2014**, *320*, 780.
[38] F. Chi, Y. Zeng, C. Liu, D. Liang, Y. Li, R. Xie, N. Pan, C. Ding, *Res. Phys.* **2020**, *18*, 103315.
[39] M. Guglielmi, G. Kickelbick, A. Martucci in *Sol-Gel Nanocomposites*, Springer, Amsterdam, Netherlands **2014**.
[40] I. A. Rahman, V. Padavettan, *J. Nanomater.* **2012**, *2012*, 132424.
[41] S. K. Park, K. D. Kim, H. T. Kim, *Colloids Surf. A* **2002**, *197*, 7.
[42] K. S. Rao, K. El-Hami, T. Kodaki, K. Matsushige, K. Makino, *J. Colloid Interface Sci.* **2005**, *289*, 125.
[43] G Schmid, Nanoparticles: From Theory to Application 2nd Ed. **2010**.
[44] J. Gao, N. Kedir, C. D. Kirk, J. Hernandez, J. Wang, S. Paulson, X. Zhai, T. Horn, G. Kim, J. Gao, K. Fezzaa, F. De Carlo, P. Shevchenko, T. N. Tallman, R. Sterkenburg, G. R. Palmese, W. Chen, *Compos., Part B* **2021**, *207*, 108565.
[45] S. A. Mahadik, M. S. Kavale, S. K. Mukherjee, A. V. Rao, *Appl. Surf. Sci.* **2010**, *257*, 333.
[46] J. Wang, Y. Wu, Y. Cao, G. Li, Y. Liao, *Colloid Polym. Sci.* **2020**, *298*, 1107.
[47] A. B. D. Cassie, S Baxter, *Trans. Faraday Soc.* **1944**, *40*, 546.
[48] R. N. Wenzel, *Ind. Eng. Chem.* **1936**, *28*, 988.

[49] P.-G. de Gennes, F. Brochard-Wyart, D. Quéré in *Capillarity and Wetting Phenomena: Drops, Bubbles, Pearls, Waves* (Eds. P.-G. de Gennes, F. Brochard-Wyart, D. Quéré), Springer, Berlin, New York **2004**, 139
[50] R. Ciriminna, A. Fidalgo, V. Pandarus, F. Béland, L. M. Ilharco, M Pagliaro, *Chem. Rev.* **2013**, *113*, 6592.
[51] P. Meti, D. B. Mahadik, K.-Y. Lee, Q. Wang, K. Kanamori, Y.-D. Gong, H.-H. Park, *Mater. Des.* **2022**, *222*, 111091.
[52] J. Malzbender, J. M. J. den Toonder, A. R. Balkenende, G. de With, *Mater. Sci. Eng.: R: Rep.* **2002**, *36*, 47.
[53] S. Zheng, J. Li, *J. Sol-Gel Sci. Technol.* **2010**, *54*, 174.
[54] T. Minami, *J. Sol-Gel Sci. Technol.* **2013**, *65*, 4.
[55] T. N. Myasoedova, R. Kalusulingam, *Coatings* **2022**, *12*, 1625.
[56] M. Aparicio, J. Mosa, *J. Sol-Gel Sci. Technol.* **2018**, *88*, 77.
[57] L. Vivar Mora, S. Naik, S. Paul, R. Dawson, A. Neville, R. Barker, *Surf. Coat. Technol.* **2017**, *324*, 368.
[58] L. Vivar Mora, A. Taylor, S. Paul, R. Dawson, C. Wang, W. Taleb, J. Owen, A. Neville, R. Barker, *Surf. Coat. Technol.* **2018**, *342*, 48.
[59] J. Kron, S. Amberg-schwab, G. Schottner, *J. Sol-Gel Sci. Technol.* **1994**, *2*, 189.
[60] V. Purcar, O. Cinteza, M. Ghiurea, A. Balan, S. Caprarescu, D. Donescu, *Bull. Mater. Sci.* **2014**, *37*, 107.
[61] D. Kumar, X. Wu, Q. Fu, J. W. C. Ho, P. D. Kanhere, L. Li, Z. Chen, *Appl. Surf. Sci.* **2015**, *344*, 205.
[62] M. De Bardi, H. Hutter, M. Schreiner, *J. Non-Cryst. Solids* **2014**, *390*, 45.
[63] B. Dal Bianco, R. Bertoncello, A. Bouquillon, J.-C. Dran, L. Milanese, S. Roehrs, C. Sada, J. Salomon, S. Voltolina, *J. Non-Cryst. Solids* **2008**, *354*, 2983.
[64] N. Carmona, M. A. Villegas, J. M. Fernández Navarro, *Thin Solid Films* **2004**, *458*, 121.
[65] F. Carmona, M. A. Villegas, J. M. Fernández Navarro, *Thin Solid Films* **2006**, *515*, 1320.
[66] A. Helebrant, I. Pekárková, *Berichte der Bunsengesellschaft für Physikalische Chem.* **1996**, *100*, 1519.
[67] L. Nikolic, L. Radonjic, *Ceram. Int.* **1998**, *24*, 547.